



Research Paper

FEM-SPG coupling modelling and reinforced soil effect of maize root-soil composite



Yiwen Yuan ^{a,b} , Mingxuan Du ^a, Yanlin Zhou ^a, Yueqian Yang ^a, Xin Zhang ^c , Shuhong Zhao ^{a,*}

^a College of Engineering, Northeast Agricultural University, Harbin, Hei Longjiang, 150030, China

^b College of Mechanical and Electrical Engineering, Heilongjiang University, Harbin, Hei Longjiang, 150080, China

^c Heilongjiang Academy of Agricultural Machinery Engineering Science, Harbin, Hei Longjiang, 150081, China

ARTICLE INFO

ABSTRACT

Keywords:

Adaptive coupling
Co-node element
In-situ direct shear
Effective circumference

Root-soil composites, formed by root stubble remaining in the field and the surrounding soil, are major factors affecting the quality of maize seeding operations under conservation tillage system. Addressing this problem requires the development of efficient stubble management equipment. A dynamic simulation model of the cutting effect of a blade is established by coupling finite element method (FEM) and smoothed particle Galerkin (SPG) models. After drawing 3D solid models, soil was discretised into SPG particles, and stubble was divided into finite meshes and given different material properties respectively based on their measured data. Based on the mechanical properties of fibre-reinforced composite material, soil and stubble model were bonded as a composite by contact setting. The coupling between FEM and SPG and the non-uniqueness problem of this contact model were dealt with by the co-nodes. Direct shear simulations at two positions of the maize root-soil composite were carried out using SPG-FEM model and verified experimentally by *in-situ* tests. Test results showed that shear stress and force predicted by SPG-FEM model were in good agreement with the measured results. The results showed that the reinforcement ability of roots to soil was related to their contact area with soil and distribution uniformity. The effective circumference was shown to be able to predict the depth of maximum shear strength of root-soil composite. These current research results are useful for improving the reliability of numerical simulations of crop root-soil composite and optimising agricultural operation components.

Nomenclature

(continued)

Abbreviations

SPG	Smoothed Particles Galerkin
COH	Cohesion shear strength at zero confinement (overburden)
DNI	Direct nodal integration
ECCEN	Eccentricity parameter for third invariant effects
FEM	Finite element method
GAMMAR	Viscoplasticity parameter
INTRMX	Maximum number of plasticity iterations
MCONT	Moisture content, %
PHIMAX	Maximum shear strength angle, rad
PWD	Influence parameters of pore water
PWKS	Pore water parameters
SPGRAV	Specific gravity of soil used to get porosity
Symbols	
Φ_K	Regular shape function
A	D-P coefficient

c	Cohesion, kPa
C	Cowper Symonds strain rate parameters
C_e	Effective circumference, mm
C_r	Total circumference of branching roots, mm
d_K	Displacement smoothing function
d_{b1}	Distance between the outermost branching root and the composite center, mm
D	Circumference of maize root-soil composite, mm
NP	Particle count
E	Young's modulus, kPa
E_p	Plastic hardening modulus, kPa
e	Eccentricity parameter for third invariant effects
F	Peak shear strength, Pa
G	Shear modulus, kPa
h	Depth from the ground surface, mm
J_2	The second invariant of deviatoric stress tensor
$K(\theta)$	Tensor plane angle function

(continued on next column)

(continued on next page)

* Corresponding author.

E-mail address: shhz@neau.edu.cn (S. Zhao).

(continued)

K	Bulk modulus, kPa
P	Hydrostatic pressure, Pa
\bar{u}^h	Meshless displacement function
<i>Greek symbols</i>	
α	The angle between the branching roots and stem of maize stubble, °
β	Hardening parameter
ϵ	Elastic strain
ϵ_p^{eff}	Effective plastic strain
$\dot{\epsilon}_{ii}$	Volumetric strain rate
θ	Angle, rad
ν	Poisson's ratio
σ	Stress, kPa
φ	Internal friction angle, rad

1. Introduction

The black soil region in Northeast China is the main area for maize production (Jiang et al., 2021; Zhang et al., 2015). To improve and sustain productivity and profitability, while protecting and enhancing the resource-base where possible, conservation tillage has been widely promoted with a focus on black soil conservation (Fang & Sun, 2017). Conservation tillage practices protect the soil by maintaining sufficient surface cover by means of a standing crop, crop residues or both. Management practices under conservation tillage can mitigate soil erosion and runoff (Seitz et al., 2019) as soil structural conditions improve (Kumar et al., 2012; Zhang et al., 2012), thereby improving water infiltration and soil water retention (Dang et al., 2018; Kassam et al., 2009; Melland et al., 2017), as well as gas exchange between the soil and atmosphere (Antille et al., 2015; Govaerts et al., 2009). However, crop stubble left on seedbed also cause some trouble for the following sowing operations. Appropriate residue management is a key factor for successful crop establishment in conservation tillage system. Before sowing, especially for maize with firmly entrenched roots in the soil, plain, notched, toothed, fluted, or bubble disc coulters or blades/hoes are usually used to cut the stubble into fragments at high-rotational speeds (Li et al., 2017). The ploughing/discing operations interact with the surface stem of stubble, underground root system, and soil.

The stem serves as the primary axis connecting the underground layers of branching roots. The root system of crops have a complex growth state underground, ultimately weaving into a huge network. As early as the 1980s, Wu et al. (1988) proposed the concept of bonding relationships between plant roots and soil. Root wedging is an important trigger of shear strength and soil structure variation (Cheng et al., 2024; Wu et al., 2022). In agriculture system, residual stubble affects soil properties, with soil with roots having a higher shear strength than soil alone (Comino & Marengo, 2010; Mickovski et al., 2011; Vannoppen et al., 2015). Meanwhile, due to the similar reinforcement effect of roots and fibres in soil, Ali and Osman (2008) have also suggested that the composite formed by roots and soil can be analysed as a natural fibre-reinforced composite material. This means that compared to soil only conditions, the root-soil composite cutting process is more complicated. Therefore, fully understanding the structural characteristics and mechanical behaviour of root-soil composites in practical operating environments has been regarded as a necessary prerequisite for optimising the structure and efficient operation of conservation tillage equipment.

Modelling of root-soil interaction is a challenge considering the differences in physical connections and properties between these two materials. There are some numerical methods that can simulate the displayed surface interactions by using Lagrange multipliers or constraints executed by interface elements. However, these models are often too complex and large-scale, which can easily lead to convergence difficulties during the calculation process (Li et al., 2017). In addition, these available root and soil models have been developed for plant growth and checking tree anchoring (Mickovski et al., 2011; Yang et al.,

2014), but lack consideration for tool cutting effects. In the cutting operation of root-soil composites, the stubble is cut off, and the soil embedded in the roots will also follow the movement of the roots. Meanwhile, the characteristics of natural composite materials also need to be achieved through contact settings. Therefore, an adequate prediction model that is capable of providing a better determination of the performance of tool will be beneficial to the design and development of tillage implements.

The increasing popularity of digital simulation in agricultural engineering is attributed to the rapid advancement of computer technology and the availability of commercial simulation tools. It can be performed at any time of the year, regardless of seasonal weather, and well validated models can provide detailed insights into the tool cutting process. The prediction of soil-tool interactions has been well established in terms of numerical simulation techniques (Aikins et al., 2021; Azimi-Nejadian et al., 2022; Barr et al., 2018; Ucgul et al., 2017), however models incorporating plant stubble still in their infancy. Among numerous numerical methods, the finite element method (FEM) has been used to simulate agricultural operation, such as the interactions between equipment and the soil (Li & Schindler, 2012; Rashidi & Gholami, 2010; Tagar et al., 2015), as well as crops (Tomobe et al., 2019, 2021; Dupuy et al., 2007), FEM is used due to its excellent performance in analysing dynamic problems of material failure and large-scale deformation (Upadhyaya & RosaWulfsohn, 2002). However, in FEM, soil is assumed to be a continuous media, thus on its own it cannot model the soil-particle scale reaction well (Chen et al., 2013). In agricultural machinery operation, the discontinuous granular nature of the soil is important (Tanaka et al., 2000). Soil granulation is beneficial for accurately describing soil particle flow (Fang et al., 2016; Foldager et al., 2022), burial between soil layers (Du et al., 2022), and furrow profile after tillage (Ucgul et al., 2014), but this option is not available in FEM. As a new discrete particle meshless method, the smoothed particle Galerkin (SPG) method has been applied to simulate particle characteristics in material deformation, such as concrete and rock impact (Lee & Kwak, 2023; Tian et al., 2022), metal grinding (Stockburger et al., 2023; Wu & Wu, 2018), and soil fragmentation (Li et al., 2022). Therefore, it is a good idea to establish a simulation model of maize root-soil composite through the coupling of FEM and SPG.

This study aims to establish a numerical model that is closest to the actual field operation to simulate the maize root-soil composite and solve the non-unique solution problem in the FEM-SPG coupling process. The analysis of the reinforced soil effect of the root-soil composite and the prediction of the maximum sheet strength depth were obtained after completing the simulation model. The current results provided in this study will enable future agricultural machinery and equipment researchers to select appropriate levels of modelling details for the required research objectives.

2. Materials and methods

2.1. Basics of SPG and adaptive coupling

The Smoothed Particles Galerkin (SPG) method proposed by Wu et al. (2015), is a meshfree Galerkin method using the direct nodal integration (DNI) technique. To address the rank-loss issue encountered with the DNI technique, the SPG method implements a strain gradient stabilisation operator. This operator is predicated on a penalty function derived from displacement smoothing theory. The displacement smoothing function can generally be expressed as:

$$\bar{u}^h(x, t) = \sum_{K=1}^{NP} \Phi_K(x) d_K(t) \quad (1)$$

where $\bar{u}^h(x, t)$ is meshless displacement, $\Phi_K(x)$ is regular shape function, $d_K(t)$ is displacement smoothing function and NP is particle count.

Typically, the displacement smoothing function differs from the

shape function. However, to improve the simplicity and efficiency of the algorithm, it can be assumed that both can be represented by the same function. For more details on the SPG method and the algorithms implemented to improve accuracy readers are directed to Wu et al. (2015, 2016, & 2020).

To better replicate the physical separation and failure of materials and address any potential difficulties with inaccurate damage accumulation in meshfree approximations used in material failure analysis, a strain-based bond failure mechanism is proposed in SPG framework to accurately record displacement discontinuities and prevent any undesired damage growth (Wu, Wu, Crawford, & Magallanes, 2017). Each SPG particle has a specific influence domain, where every connection between two particles inside this domain is characterised as a bond, similar to molecular bonds in chemistry. Fig. 1 provides a visual representation of the bond failure mechanism. The red and blue circles represent the support node 1 and 2, respectively. Bonds 2-1, 2-7, 2-8, 2-9, and 2-10 are the initial five bonds that are connected to node 2. Bonds 1-2, 1-3, 1-4, 1-5, 1-6, 1-7, and 1-10 are all connected to node 1. Assuming that the failure criteria for bond 1-2 is satisfied, then bond 1-2 is broken. Therefore, the shape function at node 1 is set to zero at node 2, i.e. $\Phi_2(x_1) = 0$, while the form function of node 2 is also set to zero at node 1, i.e. $\Phi_1(x_2) = 0$. However, $\Phi_2(x_k) \neq 0$ for $k = 7, 8, 9, 10$ and $\Phi_1(x_k) \neq 0$ for $k = 3, 4, 5, 6, 7, 10$, which means all the other bonds except bond 1-2 are still connecting. As deformation progresses, the effective plastic strain of each particle steadily increases. Consequently, the separation of two particles in pairs, known as kinematic disconnection or bond failure, is regarded as a permanent and irreversible event (Wu, Wu, & Hu, 2017). Based on the above mechanism of action, the SPG method is suitable for accurately replicating the bonding behaviour observed between loam soil particles.

The afore-introduced SPG formulation has been implemented into the commercial software LS-DYNA (Livermore Software Technology Corporation, Livermore, CA, USA). LS-DYNA is a general-purpose explicit dynamic analysis program used to analyse static and dynamic response of structures to large deformations, and its operational stages are shown in Fig. 2. In this software, the FEM mesh can be automatically converted to SPG particles by defining it on “*SECTION_SOLID_SPG (ELFORM 47)”. The interface between SPG and FEM shares common nodes. The coupling between SPG and FEM is naturally dealt by shared nodes (Wu et al., 2018). By specifically using this method, these interfaces can be firmly connected to allow for variable zoning without requiring mesh transition regions. In this study, a maize root-soil composite model is developed with FEM-SPG in the framework of LS-DYNA hydrodynamic software. The main method used in the solution is explicit time integration. A contact-impact algorithm facilitates the handling of challenging contact problems by incorporating the transfer

of force and energy across the contact interface.

2.2. Measurement of soil and maize root stubble

The composite samples used in this study were sampled in April 2023 by the five-point sampling method from the experimental farm of Northeast Agricultural University in Heilongjiang Province, China. The field soil, typical black soil (Mollisols in USDA classification), was used for this modelling, and soil is divided into inner soil and outer soil ‘layers’ with the root-soil composite as the centre. Inner soil refers to the soil adhered to the maize root system within the root-soil composite, while outer soil refers to ordinary soil outside the range of the root-soil composite. The outer soil was sampled additionally using a ring knife on the wall of pits where root-soil composites were sampled. All terrestrial ecosystems have above-ground and below-ground components (Wardle et al., 2004). Schenk and Jackson (2002) found that the differences in root size between plant growth types were largely determined by differences in above-ground size. The number and spatial distribution of maize roots are related to their above-ground stems; the larger the stem diameter, the more developed the maize below-ground root system. The diameter of the above-ground stems of 50 maize stubble are counted completely randomly in the experimental field (Fig. 3a). To determine the actual contact range between root system and soil in the simulation model, 12 undisturbed maize root-soil composite samples with a same stem diameter are collected. Fresh root-soil composite samples, obtained by excavating trenches or pits, are chosen for the purpose of traits testing. Subsequently, for parameter testing, composite samples were transported to the laboratory in individual sealed plastic buckets to prevent any external stress or damage during transportation. Structural measurements and related biomechanical tests on fresh composite samples were performed within one week (Bischetti et al., 2005).

The root-soil composite was approximately a cylinder. The maize root system is classified as a type of branching root type, and its stubble consists of three major components: stem, branching root, and capillary root. After removing soil from the stubble, the geometric and material properties of stubble are evaluated (Fig. 3d). The stems and branching roots of some samples are cut off and washed in clean water. The mechanical properties of stems and branching roots are obtained using the experimental method of Li et al. (2017). Maize normally has eight levels of branching roots. This study ignored the influence of capillary roots on root-soil interaction due to the exceedingly tiny diameter (no more than 0.3 mm) of capillary root that developed from the branching root.

In the laboratory, all soil material parameters, including cohesion, friction, Young’s modulus, and Poisson’s ratio, are determined using a standard triaxial compression apparatus (Fig. 4a). The calculation of Young’s modulus is derived from the stress-strain ($\sigma_1 - \sigma_3$) curve produced from the triaxial test, namely at zero confining pressure or uniaxial compression ($\sigma_2 = \sigma_3 = 0$), as described by Tagar et al. (2015):

$$E = \frac{100 \times \Delta(\sigma_1 - \sigma_3)}{\Delta\epsilon} \quad (2)$$

where E is Young’s modulus (kPa), $\Delta(\sigma_1 - \sigma_3)$ is the change in deviatoric pressure (kPa) and $\Delta\epsilon$ is the change in elastic strain.

Poisson’s ratio was calculated as (Tagar et al., 2015):

$$\nu = \frac{\epsilon_{1R} - \epsilon_{2R}}{\epsilon_{1A} - \epsilon_{2A}} \quad (3)$$

where ϵ_{1R} is the initial thickness of the specimen before the test (mm), ϵ_{2R} is the thickness after the test (mm), ϵ_{1A} is the initial length of the specimen before the test (mm), and ϵ_{2A} is the length after the test (mm). Referring to Zhang et al. (2023), the relevant friction parameters are measured using the friction tester shown in Fig. 4b.

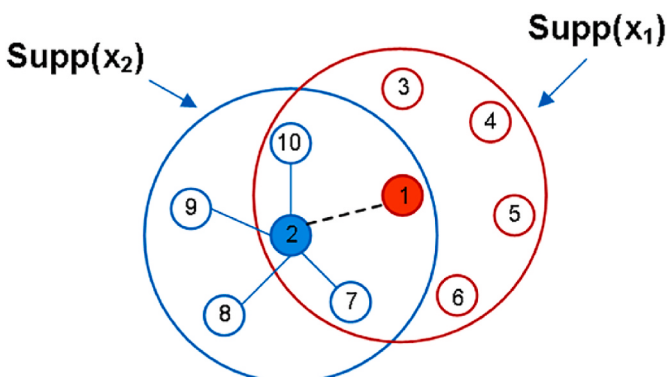
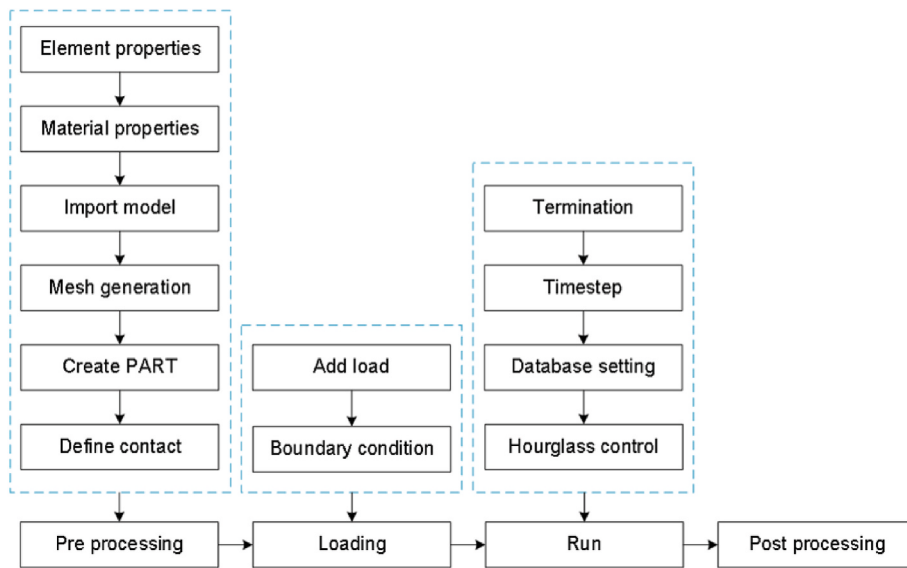
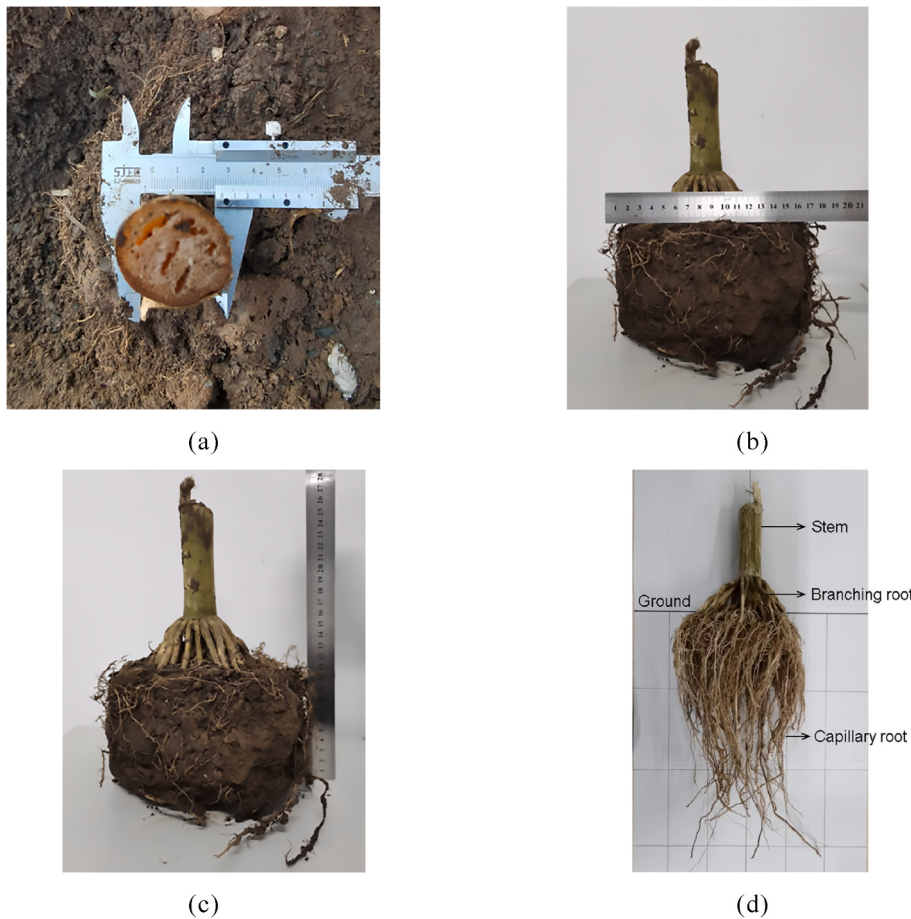


Fig. 1. – Illustration of SPG bond failure mechanism (adapted from Wu et al., 2018). The large circles marked $\text{Supp}(x_1)$ and $\text{Supp}(x_2)$ represent the support of Node 1 and 2, respectively. The solid and dashed line represent the bond and failure bond between Nodes, respectively.

**Fig. 2.** LS-DYNA simulation flowchart.**Fig. 3.** Maize root-soil composite sample structure (a) stem diameter (b) composite width (c) composite depth (d) root stubble body parts.

2.3. Modelling of root-soil composite shear system

2.3.1. Geometry modelling

The geometric morphology of maize stubble is complex. To reflect the shape and nature of the model as accurately as possible, the maize stubble model (shown in Fig. 5a), is developed in CATIA V5 software

(Dassault Systems, Suresnes, France) as followed:

- (1) Capillary roots are ignored in the modelling process.
- (2) A cylindrical tab with a diameter of 29 mm is created and the first layer branching roots are determined to be 70 mm above and 65 mm below (according to the measurements of stubble left in the

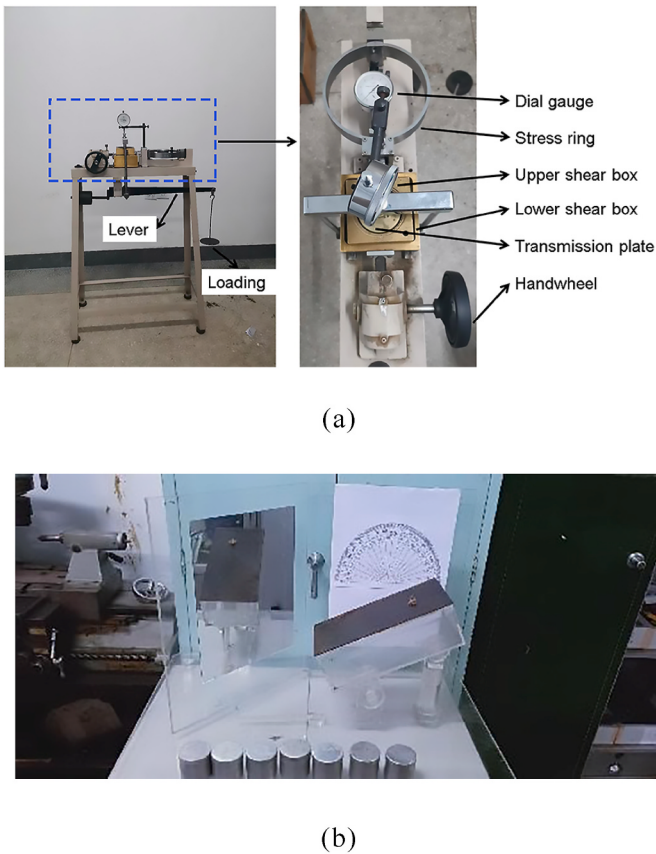


Fig. 4. – Soil physical parameters measurement device (a) direct shear apparatus, (b) friction coefficient tester.

field – see Section 3.1). The structure size of stem after removal of the branching roots at the bottom is measured and the shape of the bottom of stem is fitted by rotating slot command.

- (3) The depth from the ground surface h_1 , average angle between the bend and stem α_1 , and distance from the lowest point to the centre of stem s_1 of the outermost branching root (branching root 1 in Table 4) was measured. Sample lines are used to roughly fit the distribution pattern of branching roots. A rotating groove is used to roughly simulate the variation in branching root thickness, and a circular array is used to create an evenly distributed layer of branching roots. The steps for the rest seven layers branching roots model were the same as the first ones.

Considering the actual situation, as well as the size of maize stubble, the soil in contact or close to the root system is designated as the inner layer soil of the cylindrical model, with a base radius of 100 mm and a height of 200 mm (Fig. 5b). According to the calculation requirements of the numerical model, the soil cannot overlap with the root system, thus the maize stubble is deleted from soil by using a Boolean operation function in Catia software to ensure that no interference occurs when the soil model is assembled with the stubble model.

The above completed 3D models of stubble and soil are exported to a .stp format file. The .stp file includes data of 3D objects and provides support for product model data exchange, achieving a complete exchange of data between 3D software and meshing software.

2.3.2. Mesh generation

In this research, mesh generation is implemented using HyperMesh 2019 software (Altair, Troy, USA). Due to the irregular shape of maize stems, 15,713 3D tetrahedron element stem meshes are formed based on 2D surface quadrilateral elements. Next, the automesh technique is used

to split the finite element mesh of eight-layer branching roots, resulting in the extrusion of a mixed 2D mesh. The branching roots have a mesh size of 1 mm and a total of 124,720 elements. Subsequently, the soil's finite element mesh is generated using the linear solid approach, which includes creating a quadrilateral 2D mesh by extrusion. The mesh between stems, branching roots, and the inner soil achieves common nodes between the 2D mesh elements by associating geometric edges with grid nodes and merging grid nodes, as shown in Fig. 6. After the 2D mesh is rendered co-nodal, it is converted into 3D hexahedral mesh elements through the tetramesh function. The reason for this operation will be explained in Section 2.3.4. The inner soil SPG particles are transformed from hexahedral finite element meshes. The number of SPG particles is 109,327.

2.3.3. Material model

The LS-PrePost 4.7 software, an advanced pre and post-processor designed specifically for LS-DYNA, provides a comprehensive database that includes various material models and corresponding soil element types that may be used. The *MAT_147(MAT_FHWA_SOIL) option to use the default properties determined for soils is used here (Li et al., 2022). This is an isotropic material with damage that can be used for solid elements. This model considers various factors, such as soil viscoplastic parameters, strain reinforcement parameters, and pore water effects, ensuring that the simulation results are more realistic. The pressure-dependent peak shear strength is calculated using the modified Mohr-Coulomb surface as follows:

$$F = -P \sin \varphi + \sqrt{J_2 K^2(\theta) + A^2 \sin^2 \varphi - c \cos \varphi} = 0 \quad (4)$$

where, P is the hydrostatic pressure, φ is internal friction angle, J_2 is the second invariant of deviatoric stress tensor, $K(\theta)$ is a function of the tensor plane angle, A is the D-P coefficient, c is the cohesion.

The material properties, such as bulk density and water content of the soil model, are set from the measurement results of soil. In addition, parameters in the soil model, such as soil porosity, viscoplasticity and soil specific gravity, are set based on the reference values provided by the MAT_FHWA_SOIL model in the SPG algorithm. The influence of pore water effect on bulk modulus and effective pressure is not considered, therefore the values of PWD1, PWKSK, and PWD2 are taken as 0. GAMMAR is set as 0 to eliminate the impact of any strain rate increase on strength. In addition, ECCEN (abbreviated as e) is the eccentricity parameter of the third variable step, which changes the shape of the yield surface through the standard Mohr-Coulomb $K(t)$ equation. When $e = 0.55$, the yield surface becomes a triangular conical; when $e = 1$, the yield surface becomes conical. The yield surface equation is shown in Eq. (5):

$$K(\theta) = \frac{4(1 - e^2)\cos^2 \theta + (2e - 1)^2}{2(1 - e^2)\cos \theta + (2e - 1)\sqrt{4(1 - e^2)\cos^2 \theta + 5e^2 - 4e}} \quad (5)$$

$$\text{where } \cos 3\theta = \frac{3\sqrt{3}J_2}{2\sqrt{J_2}}, \quad 0.5 < e \leq 1.$$

In this study, to ensure the smoothness of the yield surface and to meet the shape condition of the yield surface, the final value of e in this study is 0.7 (Li et al., 2022). In addition to the main soil parameter values shown in Table 1, the default values corresponding to MAT_FHWA_SOIL materials are used for all other parameters.

According to the mechanical properties of the stems and branching roots tested in Li et al. (2017), it is evident that the stem and branching roots both meet the characteristic standards of elastic-plastic materials. However, their stress-strain curves are not identical. According to LS-DYNA Keyword User's Manuals (LSTC, 2018), the *MAT_003 (MAT_PLASTIC_KINEMATIC) and *MAT_012(ISOTROPIC-ELASTIC-PLASTIC) functions are selected as the material for the stem and branching roots, respectively, in the simulation tests. The *MAT_003 (MAT_PLASTIC_KINEMATIC) material model is ideal for simulating both

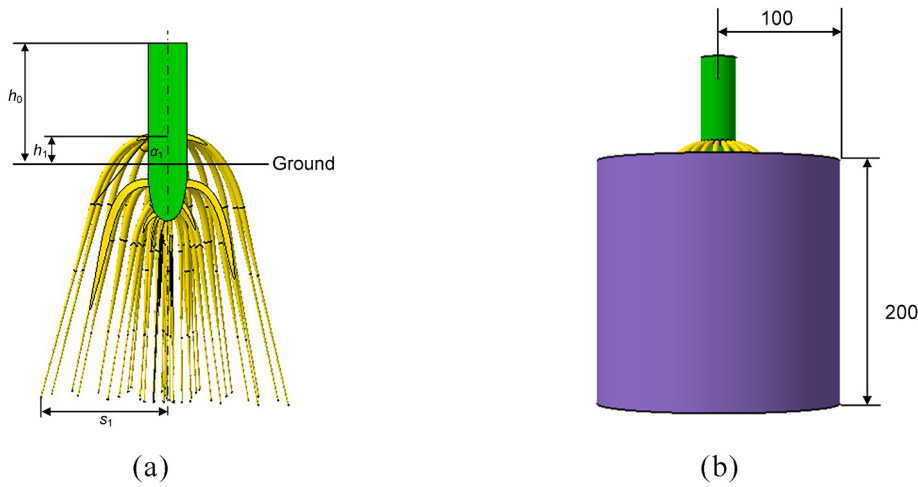


Fig. 5. – Geometric model of Catia (a) maize root stubble profile (b) root-soil composite with inner layer soil.

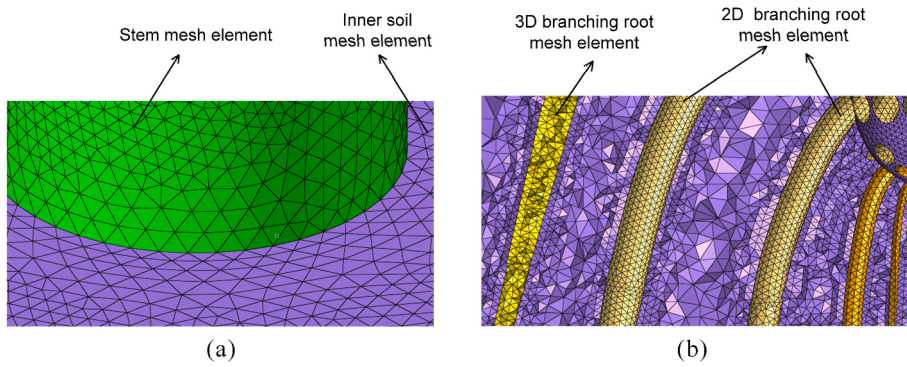


Fig. 6. –Local sectional view of common node mesh elements between maize stubble and soil: (a) soil and stem; (b) 3D mesh elements transformed from 2D mesh elements of branching root.

Table 1
Soil property parameters used in SPG simulation.

Parameters	Inner soil	Outer soil
Specific gravity of soil used to get porosity, SPGRAV	2.64	2.43
Viscoplasticity parameter (strain-rate enhanced strength), VN	1.2	1.1
Maximum number of plasticity iterations, INTRMX	10	10
Bulk modulus (non-zero), K (MPa)	7.96	6.48
Shear modulus (non-zero), G (MPa)	1.34	1.24
Peak shear strength angle (friction angle) (radians), PHIMAX (rad)	0.435	0.426
Cohesion n shear strength at zero confinement (overburden), COH (MPa)	4.7	4.5
Eccentricity parameter for third invariant effects, ECCEN	0.7	0.7
Moisture content of soil (determines amount of air voids) (0-1.00), MCONT	0.2134	0.2012

isotropic and kinematic hardening plasticity, with the added capability of include rate effects. This model offers superior accuracy and has its own failure parameters. The plastic behaviour is defined by a tangent modulus, but the strain rate effects are not considered in the model. The equation for yield stress is as follows:

$$\sigma_y = \left[1 + \left(\frac{\dot{\varepsilon}}{C} \right)^{\frac{1}{P}} \right] \left(\sigma_0 + \beta E_p \varepsilon_p^{\text{eff}} \right) \quad (6)$$

where $E_p = E_{\tan} E / (E - E_{\tan})$ is the modulus of plasticity hardening, $\dot{\varepsilon}$ is the strain rate, C and P are Cowper Symonds strain rate parameters, σ_0 is the

initial yield stress, β is the hardening parameter, E_p is the plastic hardening modulus, $\varepsilon_p^{\text{eff}}$ is the effective plastic strain.

The material model used for the branching roots is *MAT_012/ISOTROPIC-ELASTIC-PLASTIC. This material represents the isotropic plasticity of 3D solids at an extremely low cost. Here the pressure p is integrated in time:

$$\dot{p} = -K\dot{\varepsilon}_{ii} \quad (7)$$

where K is the bulk modulus and $\dot{\varepsilon}_{ii}$ is the volumetric strain rate.

The stubble property parameters utilised in the simulation are determined based on the measured material parameters (see Section 3.1) and the literature (Yuan et al., 2023).

2.3.4. Contact relationship setup

The modelling of root-soil interactions is a crucial and challenging aspect in the modelling process of root-soil composites. This is due to the intricate physical connection between the root and soil phases, as well as the differences in their characteristics. In LS-DYNA, a contact is defined by identifying (via parts, part sets, segment sets, and/or node sets) what locations are to be checked for potential penetration of a slave node through a master segment. In previous research on fibre-reinforced composite materials, it was found that there was a thick interfacial layer between fibres and matrix, which transmits stress to enhance the entire composite material (Bian et al., 2018; Budiman et al., 2016; Upadhyaya & Kumar, 2015). The contact interface plays an important role in the increase of soil strength by the root system. The relative displacement between soil and stubble is small, with most of the soil

trapped in the root system (Li et al., 2017). This is in line with the *CONTACT_TIED_OPTION function in LS-DYNA (Dupuy et al., 2007; Temgoua et al., 2016). In tied contact, the slave nodes are constrained to move with the master surface. According to the FEM calculation requirements, underground root segments are designed as a master surface, and soil nodes are slave nodes. A stress transfer interface is formed at the “tied” contact between soil and roots. At the beginning of the simulation, the nearest master segment for each slave node is located based on an orthogonal projection of the slave node to the master segment. If the slave node is considered close to the master segment, the slave node will be moved onto the master surface. In this way, the isoparametric position of the slave node with respect to its master segment is held fixed using kinematic constraint equations. However, due to the robustness limitations of this method, non-unique solutions may occur when used for geometrically complex problems (Tomobe et al., 2019). To solve this problem, soil meshes are divided through co-nodes after generation of root meshes in the pre-treatment, thereby determining the master segments that can be selected by slave nodes. The coupling between the FEM stubble and the SPG soil particles is dealt with by the shared nodes. The range of the tied contact is set to be equal to the average diameter of the root-soil composite in the stubble sample, which is measured at 200 mm.

2.4. In-situ shear test

2.4.1. Physical tests

It is difficult to reproduce the root structure in the soil after digging out plants, especially for fine roots. To determine the validity of the simulated model and explore the reinforced soil effect of maize root-soil composite, direct shear tests are conducted on an electronic universal testing machine (RGM-2050, Reger Instruments Co. Ltd, China, shown as Fig. 7a). There is no standard to follow for shear tests of maize root-soil composites. In this test, a shear test is designed with reference to shear testing machines for other materials, including a fixture installed on an electronic universal testing machine for *in-situ* shear testing. Fig. 7b shows the geometrical structure of shear tool. In production operations, most of the edges of tillage components are curved rather than straight, so the cutting edge of the shear blade is designed as a

circular arc to simulate actual operation. The shear tool is made of 65Mn steel, with a width of 100 mm and a thickness of 5 mm. The inclination angle is 30° with a single edge. Maize stubble are surrounded by the field soil, and when sheared, the surrounding soil exerts compressive pressure. To maintain consistency with the field situation as much as possible, the plastic bucket that the composite is packaged in is clamped onto the test bench (Fig. 7a). To avoid an offset of the cutting blade, the cutting speed is set to 120 mm min⁻¹. Zhang et al. (2023) concluded that there is a significant difference in the ultimate shear force applied to a shear blade at different distances from the centre of the root system. Therefore, the shear positions are at the centre and 40 mm away from the centre of stubble, corresponding to positions I and II in Fig. 7c, respectively. The pure outer soil samples including the control group are subjected to six repeated shear tests.

2.4.2. Simulated tests

In the physical test, the plastic bucket containing the root-soil composite sample underwent some deformation after the shear blade cut into the composite. To avoid an ‘explosion’ of simulated SPG particles and to keep the internal compression pressure of root-soil composite consistent with the physical tests, a gap of 2 mm is left between the composite and the outer soil. Although the shape of the outer soil did not match the physical tests, the outer soil is drawn as a hollow rectangle matching the dimensions of the composite and taking into consideration the boundary settings of simulation tests and the fact that the shear object did not include the outer soil.

Fig. 8a shows the geometric structure size of simulation model. The SPG particles of the outer soil are transformed from hexahedral meshes by line drag methods which extrude the surface meshes. To shorten the simulation time, as the outer soil mainly plays a fixed role, the mesh sizes of the outer soil is set at 10 mm, and the number of hexahedron elements is 16000. The whole maize root-soil composite for the *in-situ* shear test model, shown in Fig. 8b, has 152,722 nodes and 801,328 3D solid elements. Compared to the stubble, the blade is very hard and wear during operation is neglected in this study, so the blade is treated as rigid. The outer soil is set to be the same material as root-soil composite soil (i.e. inner soil), and its specific parameters in simulation tests are displayed in Table 3.

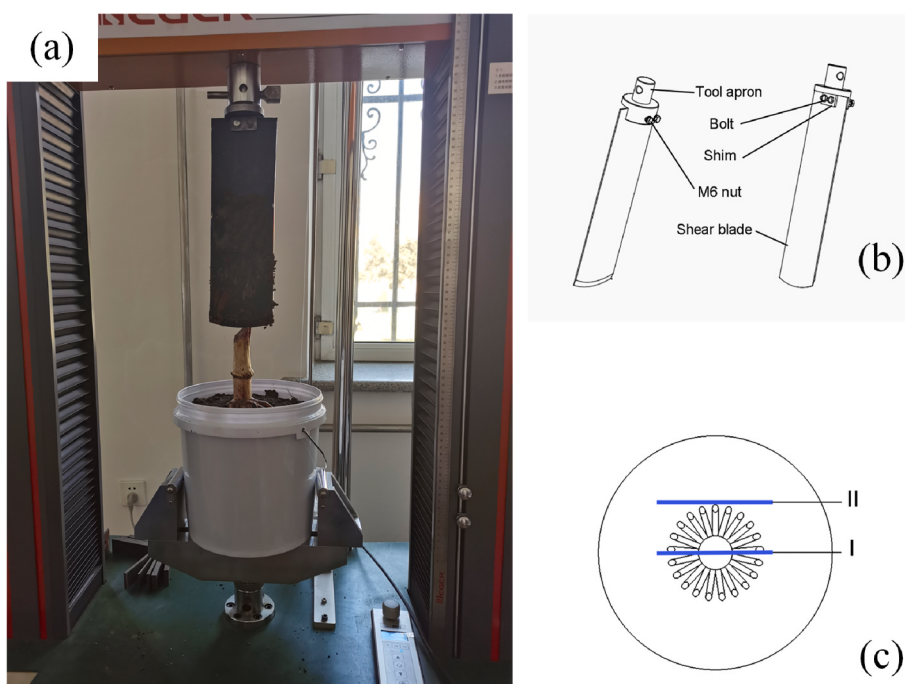


Fig. 7. In-situ shear test (a) samples and universal testing machine (b) assembly diagram of self-made cutting tools (c) shear position.

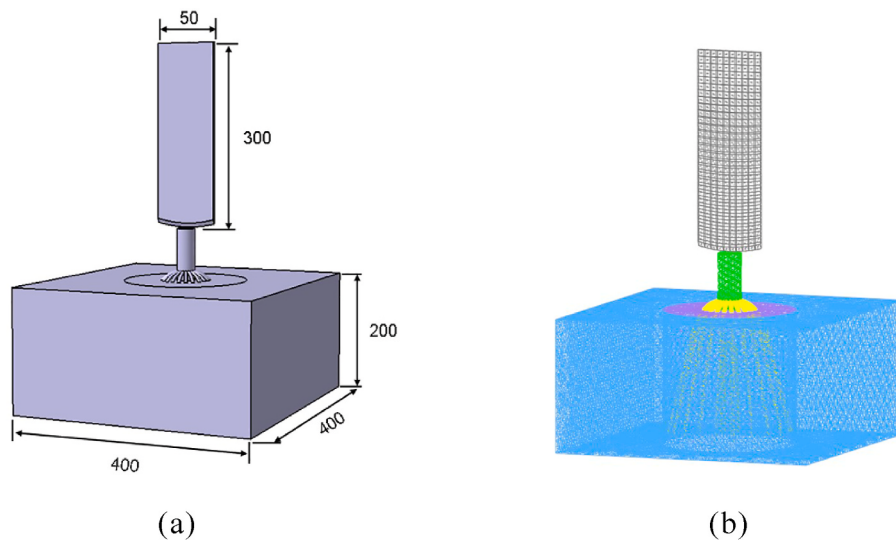


Fig. 8. – Simulated shear test of maize root-soil composite (a) geometric model and (b) 3D mesh generation of maize root-soil composite.

Table 2

– Key parameters used in simulated shear test.

Objects	Parameters	Values
Shear blade	Material	MAT_RIGID
	Elastic modulus (MPa)	1.96×10^5
	Shear modulus (MPa)	7.9×10^4
	Poisson's ratio	0.3
Soil-blade	Coefficient of static friction	0.313
	Coefficient of rolling friction	0.107
Straw-blade	Coefficient of static friction	0.3
	Coefficient of rolling friction	0.01
Stubble-blade	Coefficient of static friction	0.6
	Coefficient of rolling friction	0.02

Table 3

Main properties of soil.

Parameters	Value	
	Inner soil	Outer soil
Bulk density (kg m ⁻³)	2640	2150
Cohesion (Pa)	68500	49860
Moisture (%)	21.34	20.32
Internal friction angle (rad)	0.435	0.426
Elastic modulus (MPa)	3.82	3.5
Bulk modulus (MPa)	7.96	6.48
Shear modulus (MPa)	1.34	1.24
Poisson's ratio	0.42	0.41

In the shear simulation, due to significant deformation of the model, it is not always possible to predict the direction of parts relative to each other. In LS-DYNA, automatic contact is used to check for penetration on

either side of the casing components (Fig. 9). The contacts between shear blade and stubble and soil are defined by *CONTACT_AUTOMATIC_SURFACE_TO_SURFACE. The friction parameters are shown in Table 2.

The degrees of freedom in all directions of elements in the bottom surface of the soil part are limited. In the Y and X direction, the *BOUNDARY_SPC_SET function imposes constraints on the outer soil surfaces. The implementation of a non-reflecting boundary condition is done to limit the impact of wave reflections at the boundary. Furthermore, the shear blade is set to the same falling speed as the actual shear test in order to validate the simulation model. Fig. 10 shows the simulation models of shear root-soil composite and soil only, respectively.

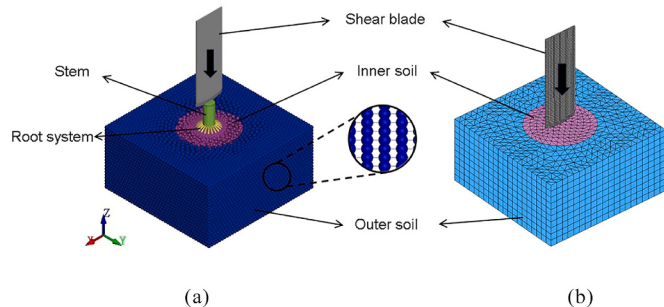


Fig. 10. Simulation model of direct shear tests (a) root-soil composite (shaded element mode) and (b) soil only (view element mode).

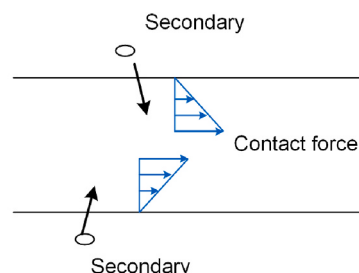
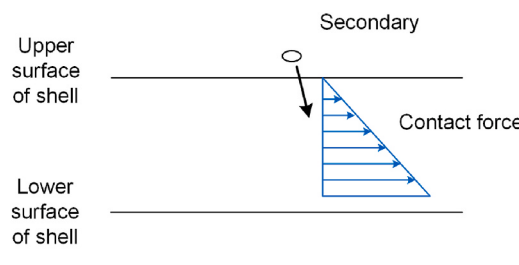


Fig. 9. Automatic and non-automatic contact.

3. Results and discussion

3.1. Results of physical measurement

Based on the results of the soil direct shear, drying and bulk density determination test, the main properties of the stubble were calculated, as shown in [Table 3](#). The average diameter of the above-ground stems of maize root-soil composite was 29 mm. The width range of under-ground roots was 180–220 mm, while their depth ranged from 100 to 180 mm. The structure and mechanical properties of stems and branching roots are shown in [Table 4](#).

3.2. Comparison of simulation model with shear tests

For the physical shear test, the load received by sensors in the vertical direction of shear blade was used as the evaluation index. The measured force and shear displacement data are plotted as scatter plots and polynomial fitted curves, and compared with the simulated curve, as shown in [Fig. 11](#). When shearing soil only particles, the curve was smoother due to the single material, and the simulation values showed a good correlation with the measured values. In contrast, the shear force changes at site I and II increased in steps when cutting the stem and branching roots. Although there was still a certain gap between the simulation values and the measurement data, it can be clearly seen in [Fig. 11b](#) and c that they showed almost the same trend. The 95 % prediction interval in light red was plotted based on the curve fitted by measured values, and the simulation numerical curves were mostly located within this interval. This demonstrated that the model could accurately replicate the shear operation of root-soil composite.

In the shear tests, the maximum shear force was the most important indicator. Throughout the entire shearing process, the shear force constantly changed, and it was not possible to guarantee that the simulation results and actual experiments would achieve good consistency at every moment. It was also difficult to compare the magnitude of shear force at each time step. Thus, the maximum and average shear force acting on the shear blade along the Z axis were the focus of this work. A comparison between simulated and test measurements is shown in [Fig. 12](#). For soil only tests, the maximum shear forces required for the simulated and physical measurements were 221.61 N and 200.1 N, respectively, with a relative error of 10.75 %. Meanwhile, the relative error of their average shear force during the shearing process was relatively low, at 8.74 %. It is concluded from this result that the soil simulation can predict real field soil properties and predict tillage force during operation. Due to the anisotropy and the complexity of plant materials in the field, and there are no plants that grow exactly the same, the predicted error values were slightly lower for the root-soil composite tests than for that of soil only tests. The length of the above-ground stems was not exactly the same, so the data from stem cutting was omitted

when processing the data at site I. The relative error between the simulated and measured values of the maximum shear force during root cutting was relatively large, at 18.1 % and 20.13 %, respectively. For plants, there may be significant differences between plants in their attribute parameters ([Zhang et al., 2020](#)). Nevertheless, the error of average shear force between simulated and physical measured values was <10 %, indicating that model had enough accuracy when simulating working performance of tillage tools that deal with plant stubble. Thus, it can be concluded that the maize root-soil composite model, implemented using the FEM-SPG coupling method, exhibited a strong correlation with actual *in-situ* direct shear tests, which means that the proposed simulation method is reasonable and applicable.

3.3. Study on the shear performance of root-soil composite

3.3.1. The effect of shear position on the ultimate shear stress

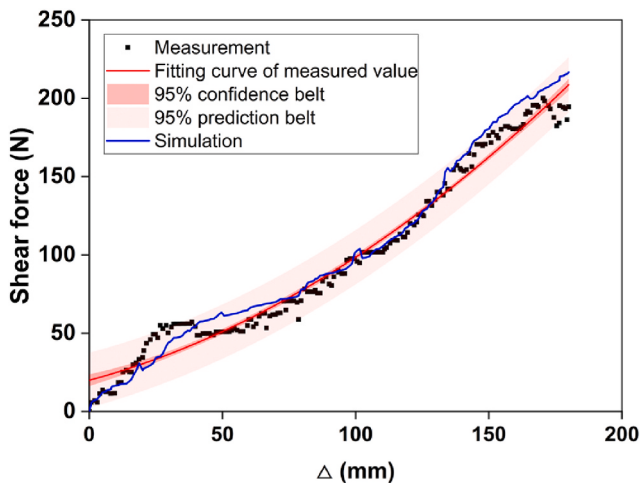
[Fig. 13](#) shows the shear stress peak of the root-soil composite at different shear positions. The shear stress peak of the four root-soil composite samples at site II was greater than that at site I. This phenomenon was mainly determined by the distribution of branching roots ([Fig. 4b](#)). From the perspective of composite materials, maize root-soil composite can be seen as reinforced soil, and branching roots can be seen as natural flexible reinforced material. The branching roots of maize stubble were closely integrated with the soil. The branching roots and their lateral roots crisscross, forming a cylindrical multi-layer cage shaped root-soil composite, which effectively enhance the shear stress resistance of root-soil composite. The size root system was approximately conical in shape, and the distribution was the most developed in the longitudinal interface of site II. The shear direction was approximately perpendicular to the growth direction of branching roots. A large number of branching roots needed to be shorn, so the peak shear stress at site II was the highest; At site I, the cutting direction was consistent with the fibre direction of the stem and the growth direction of the branching roots. Consequently, the shear strength enhancement of the root-soil composite was not significant here, so the peak shear stress at site I was smaller than at site II. It was also noted that the farther away the longitudinal shear profile was from the centre of the stubble, the sparser the branching roots, the smaller the root-soil bonded force, and the lower the peak shear force.

3.3.2. The relationship between shear stress and longitudinal depth

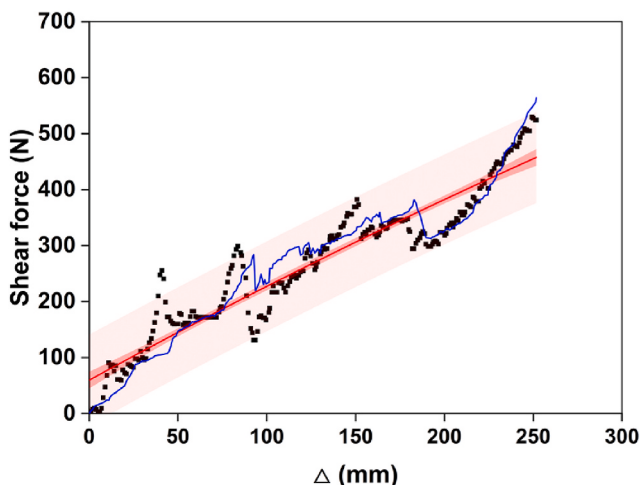
The typical shear stress-displacement relationship curves of the tested root-soil composite and soil only samples are shown in [Fig. 14](#). There was no general law that can describe the soil reinforcement effect of root system in the values of shear data from soil only and root-soil composite samples. There was a lot of variability, even when the samples were taken from the same experimental area, due to various factors including their chemical and physical characteristics and the

Table 4
Geometric and characteristic properties of maize stubble.

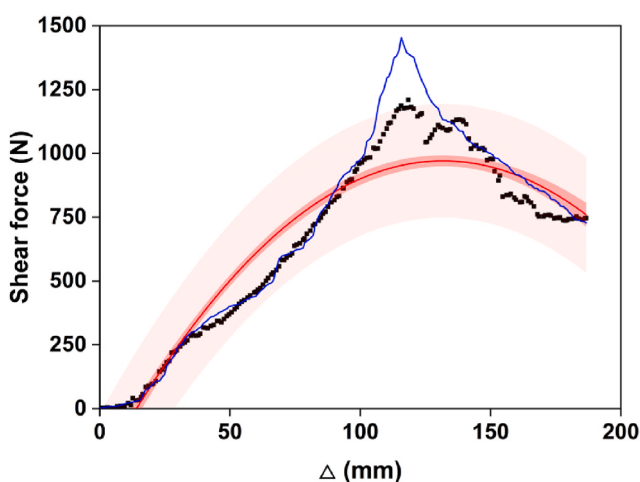
Property	Value								
	Stem	Branching root level							
		1	2	3	4	5	6	7	8
Mean diameter (mm)	29	5	6	5	4	3	2	1	1
Amount	–	21	16	13	7	7	4	4	1
Depth <i>h</i> (mm)	–84	–14	6	35.5	42	44.5	46	47.5	48.5
Distance <i>s</i> (mm)	–	91	80	73	68	59	40	32	0
Angle θ (°)	–	79	85.5	51.5	64.2	48.2	19.4	20.5	0
Bulk density (kg·m ^{–3})	202.64	264.13	256.13	238.67	264.13	264.98	264.98	264.98	264.98
Elastic modulus (MPa)	280	109	131	149	582	582	582	582	582
Poisson's ratio	0.3	0.3	0.3	0.3	0.3	0.3	0.3	0.3	0.3
Yield stress (MPa)	12	1.5	2.2	4.7	14.3	14.3	14.3	14.3	14.3
Shear modulus (MPa)	–	41.92	50.38	57.36	223.85	223.85	223.85	223.85	223.85
Plastic hardening modulus (MPa)	–	0.65	0.65	0.65	0.65	0.65	0.65	0.65	0.65
Bulk modulus (MPa)	–	90.83	109.17	124.17	485	485	485	485	485



(a)



(b)



(c)

Fig. 11. Comparison of physical and simulation load- Δ (displacement) curve (a) pure soil (b) site I and (c) site II.

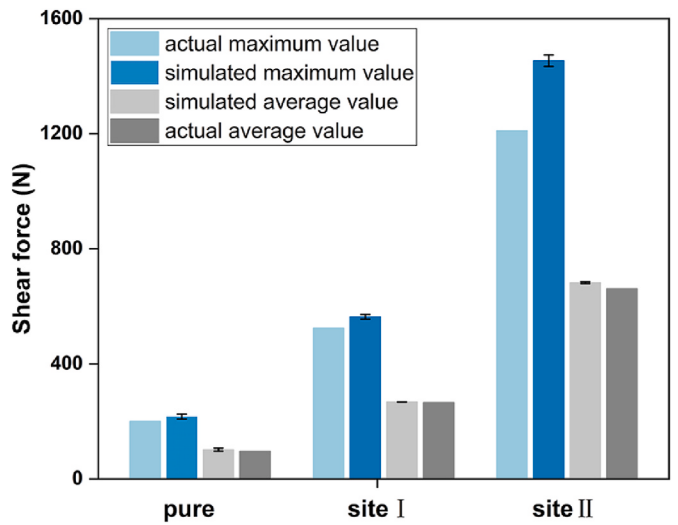


Fig. 12. – Comparison shear force of physical and simulated tests.

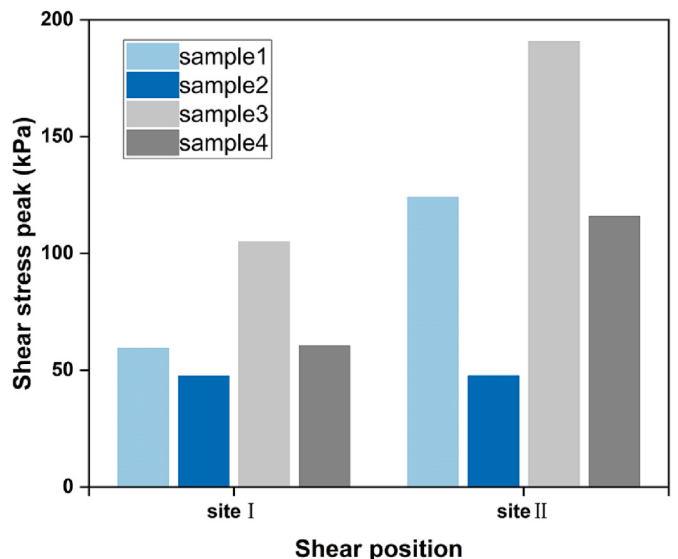


Fig. 13. – The effect of shear profile position on the shear stress peak of root-soil composite.

randomisation of crop root growth due to different soil particles densities and the presence of voids. Despite the variability of the data, overall trends were identified. The increase in shear stress of the composite samples was evident as the displacement increased, while it was not significant in the soil only sample. The increase in shear stress stopped when it reached the peak value, which represented the maximum shear stress of the material, even though all samples did not reach their maximum shear stress at the same time. Meanwhile, the peak shear stress of the root-soil composite samples was higher than that of the soil only samples, i.e. the root-soil composites required a greater force to break than soil only samples.

The shear stress varied non-linearly with longitudinal depth. At a longitudinal depth of 0–100 mm, the shear stress first increased sharply, reached its maximum value, and then oscillated slightly within a certain depth range (100–150 mm). Generally, the maximum shear stress occurred at a longitudinal depth of 100–150 mm. To identify the reason for the depth of the peak shear stress, profile processing was conducted on the root-soil composite solid model at the depth of peak occurrence and other random depths (Fig. 15).

Compared with the depth at which peak shear stress occurred,

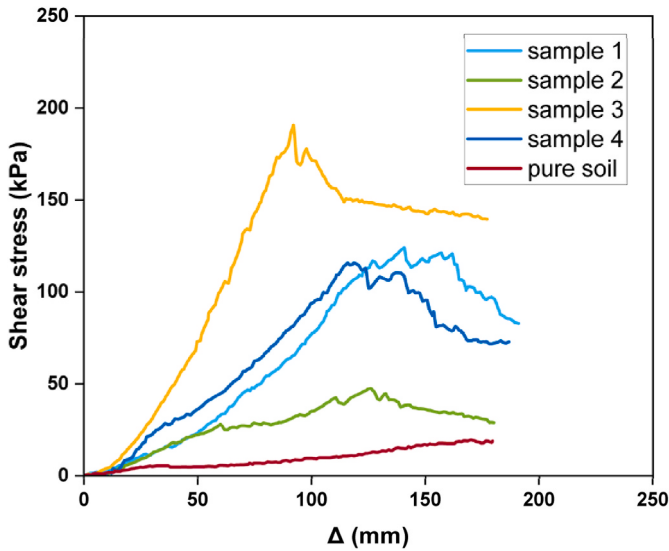


Fig. 14. – Representative stress- Δ (displacement) curves of in-situ shear tests in site II.

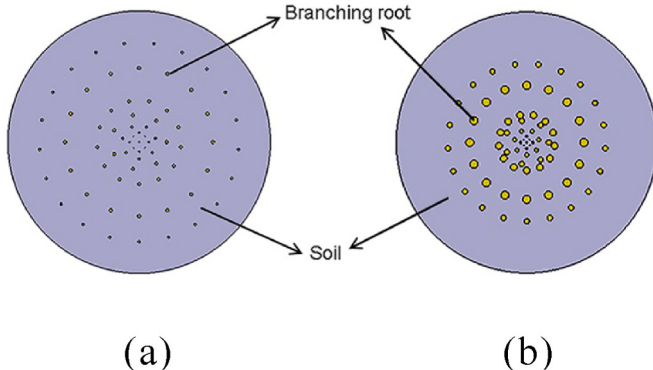


Fig. 15. Horizontal profile of root-soil composite at different depths (a) 116 mm (the position where the peak shear stress occurs of simulation) (b) 55 mm.

branching roots at a depth of 55 mm were congregated at the centre of the complex with a higher density of root distribution. In contrast, branching roots at a depth of 116 mm were evenly distributed across the profile in a dispersed manner with a less dense distribution. Ma'ruf (2012) demonstrated experimentally that root distribution density affects soil shear strength. As the depth increased, maize branching roots showed a progressively thinner growth pattern, with different root contact areas with the soil. From this, it can be seen that the uniformity of root distribution and the contact area between roots and soil (represented by the circumference on the horizontal profile) may be the reasons affecting the peak shear stress. Therefore, a new evaluation indicator for effective circumference C_e , can be calculated by Eq. (8):

$$C_e = \frac{C \cdot d_{b1}}{D} \quad (8)$$

where C_e is effective circumference, which is the circumference of the root system that has a reinforcing effect on the soil at a certain depth (mm); C is the total circumference of all branching roots of a composite on a horizontal profile at a certain depth (mm); d_{b1} is the distance between the outermost branching root and the centre of the composite (mm); and D is the circumference of maize root-soil composite, $D = 200$ mm. To further validate this conclusion, the total circumference values and effective circumference of branching roots at each depth were extracted at 10 mm intervals and plotted as Fig. 16.

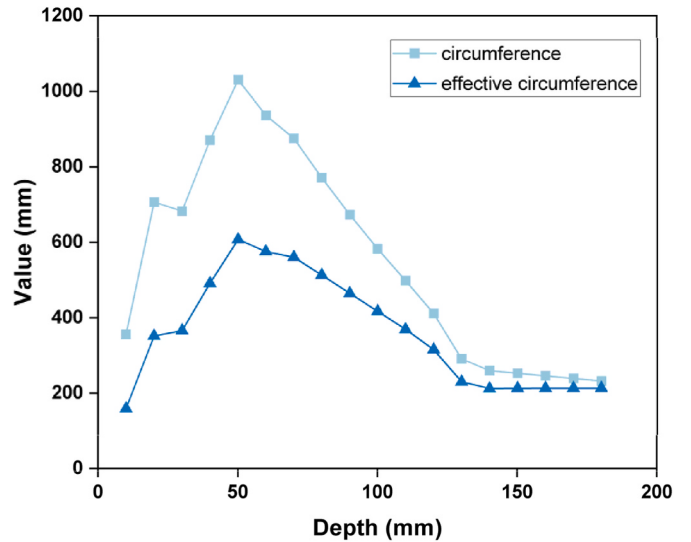


Fig. 16. Value of circumference of branching roots with depth variation.

As the depth increased, the trend of changes in root circumference and effective circumference were basically the same, showing an overall trend of first increasing and then decreasing. Therefore, it can be assumed that the root diameter dominated among the factors affecting the shear strength of composite. For a single root, the thicker the root, the larger the contact area with soil, the greater the formation of the shear stress transmission interface, which can achieve relatively good soil reinforcement effect. This is consistent with the theory of friction reinforcement. This conclusion suggests that the root system maintained the stability of the root-soil composite in the soil by its own tensile strength and the friction generated by the interaction between roots and the soil. The larger the root-soil contact area, the greater the friction generated within a root-soil composite (Yan et al., 2010). Similarly, Su et al. (2022) also showed that changes in soil mechanical properties mainly occurred in the root-soil contact surface, with root length and diameter determined by root surface area. However, the maize root-soil composite has multiple branching root within it, and its soil reinforcement effect is realised through the joint action of all branching roots. Therefore, it is necessary to consider the internal root distribution.

The maximum value of circumference was reached at a depth of 50 mm (1030.466 and 607.480 mm for circumference and effective circumference, respectively). At this depth, the root-soil contact area reached its maximum; however, the shear strength was not equally maximised. This is because the depth of the root system here is relatively shallow, and all roots gather and grow around the centre. The degree of root consolidation is only approximately half of the entire composite ($d_{b1} = 58.592$ mm). As the depth continued to increase, the circumference value decreased until the depth reached 120 mm, when the circumference value stabilised. When the depth reached 120 mm, the reinforcement effect of root system on soil reached a saturated state. Therefore, during the direct shear test, the shear stress should reach its maximum value at this depth. This was basically consistent with the simulation results (peak at 116 mm). For agricultural operations in stubble management, splitting or breaking of stubble is currently the main objective. The advance prediction of shear strength at different depths of root-soil composite will play an important role in the design of stubble cutting tools and the optimisation of operational parameters. This will be the next research step to be performed.

4. Conclusion

This study developed a feasible maize root-soil composite model using the FEM-SPG coupling method to simulate the true state of maize

stubble left after harvest under conservation tillage. The geometric shapes of soil and stubble were restored and assembled into a composite through 3D model. To verify the accuracy of the simulation model, *in-situ* shear tests were conducted on root-soil composites. The test results indicated that the simulated and physically measured shear force showed almost the same trend, while the simulated curve lay predominantly within the 95 % prediction interval plotted on the basis of the curve fitted to the measured values. The error values for the maximum and average values of the predicted shear force were likewise within acceptable limits.

The simulated results were combined with physical measurements to analyse the effect of position and depth on the shear performance of root-soil composite. In combination with the shear stress change curve during the shear blade drop, the effective circumference was proposed as an indicator to predict the depth at which the maximum shear strength of the root-soil composite occurred. It was illustrated that in a maize root-soil composite, the area of root contact with the soil and the uniformity of root distribution jointly affects its shear strength. The further development of this work considers simulating agricultural operations with different implements using the maize root-soil composite SPG-FEM model to assist in the design and optimisation of agricultural equipment and their operation parameters for conservation tillage.

CRediT authorship contribution statement

Yiwen Yuan: Writing – review & editing, Writing – original draft, Software, Methodology, Funding acquisition, Formal analysis, Data curation, Conceptualization. **Mingxuan Du:** Visualization, Software. **Yanlin Zhou:** Visualization, Software. **Yueqian Yang:** Validation, Supervision. **Xin Zhang:** Writing – original draft, Resources. **Shuhong Zhao:** Writing – review & editing, Project administration.

Declaration of competing interest

We declare that we have no known competing financial interests or personal relationships that could have appeared to influence the work reported in this paper.

Acknowledgements

This study was supported by the "Unveiling and Leading" Technology Research and Development Project of Heilongjiang Province (Grant No. 2021ZXJ05B03).

References

- Aikins, K. A., Barr, J. B., Antille, D. L., Ucgul, M., Jensen, T. A., & Desbiolles, J. M. (2021). Analysis of effect of bentleg opener geometry on performance in cohesive soil using the discrete element method. *Biosystems Engineering*, 209, 106–124. <https://doi.org/10.1016/j.biosystemseng.2021.06.007>
- Ali, F. H., & Osman, N. (2008). Shear strength of a soil containing vegetation roots. *Soils and Foundations*, 48(4), 587–596. <https://doi.org/10.3208/sandf.48.587>
- Antille, D. L., Chamen, W. C. T., Tullberg, J. N., & Lal, R. (2015). The potential of controlled traffic farming to mitigate greenhouse gas emissions and enhance carbon sequestration in arable land: A critical review. *Transactions of the ASABE*, 58(3), 707–731. <https://doi.org/10.13031/trans.58.11049>
- Azimi-Nejadian, H., Karparvarfar, S. H., & Naderi-Boldaji, M. (2022). Weed seed burial as affected by mouldboard design parameters, ploughing depth and speed: DEM simulations and experimental validation. *Biosystems Engineering*, 216, 79–92. <https://doi.org/10.1016/j.biosystemseng.2022.02.005>
- Barr, J. B., Ucgul, M., Desbiolles, J. M. A., & Fielke, J. M. (2018). Simulating the effect of rake angle on narrow opener performance with the discrete element method. *Biosystems Engineering*, 171, 1–15. <https://doi.org/10.1016/j.biosystemseng.2018.04.013>
- Bian, P. L., Qing, H., & Gao, C. F. (2018). Micromechanical analysis of the stress transfer in single-fiber composite: The influence of the uniform and graded interphase with finite-thickness. *Applied Mathematical Modelling*, 59, 640–661. <https://doi.org/10.1016/j.apm.2018.02.023>
- Bischetti, G. B., Chiaradia, E. A., Simonato, T., Speziali, B., Vitali, B., Vullo, P., & Zocco, A. (2005). Root strength and root area ratio of forest species in lombardy (Northern Italy). *Plant and Soil*, 278(1), 11–22. <https://doi.org/10.1007/s11104-005-0605-4>
- Budiman, B. A., Triawan, F., Adzman, F., & Nurprasetio, I. P. (2016). Modeling of stress transfer behavior in fiber-matrix composite under axial and transverse loadings. *Composite Interfaces*, 24(7), 677–690. <https://doi.org/10.1080/09276440.2017.1262666>
- Chen, Y., Munkholm, L. J., & Nyord, T. (2013). A discrete element model for soil-sweep interaction in three different soils. *Soil and Tillage Research*, 126, 34–41. <https://doi.org/10.1016/j.still.2012.08.008>
- Cheng, P., Wu, L., Zhang, H., & Zhou, J. (2024). Inclusion of root water absorption and reinforcement in upper bound limit stability analysis of vegetated slopes. *Computers and Geotechnics*, 169, Article 106227. <https://doi.org/10.1016/j.compgeo.2024.106227>
- Comino, E., & Marengo, P. (2010). Root tensile strength of three shrub species: Rosa canina, Cotoneaster dammeri and Juniperus horizontalis: Soil reinforcement estimation by laboratory tests. *Catena*, 82(3), 227–235. <https://doi.org/10.1016/j.catena.2010.06.010>
- Dang, Y. P., Balzer, A., Crawford, M., Rincon-Florez, V., Hongwei, L., Melland, A. R., et al. (2018). Strategic tillage in conservation agricultural systems of north-eastern Australia: Why, where, when and how? *Environmental Science and Pollution Research*, 25, 1000–1015. <https://doi.org/10.1007/s11356-017-8937-1>
- Du, J., Heng, Y., Zheng, K., Luo, C., Zhu, Y., Zhang, J., & Xia, J. (2022). Investigation of the burial and mixing performance of a rotary tiller using discrete element method. *Soil and Tillage Research*, 220. <https://doi.org/10.1016/j.still.2022.105349>. Article 105349.
- Dupuy, L. X., Fourcaud, T., Lac, P., & Stokes, A. (2007). A generic 3D finite element model of tree anchorage integrating soil mechanics and real root system architecture. *American Journal of Botany*, 94(9), 1506–1514. <https://doi.org/10.3732/ajb.94.9.1506>
- Fang, H., & Sun, L. (2017). Modelling soil erosion and its response to the soil conservation measures in the black soil catchment, Northeastern China. *Soil and Tillage Research*, 165, 23–33. <https://doi.org/10.1016/j.still.2016.07.015>
- Fang, H., Zhang, Q., Chandio, F. A., Guo, J., Sattar, A., Arslan, C., & Ji, C. (2016). Effect of straw length and rotavator kinematic parameter on soil and straw movement by a rotary blade. *Engineering in Agriculture, Environment and Food*, 9(3), 235–241. <https://doi.org/10.1016/j.eaef.2016.01.001>
- Foldager, F. F., Munkholm, L. J., Balling, O., Serban, R., Negrut, D., Heck, R. J., & Green, O. (2022). Modeling soil aggregate fracture using the discrete element method. *Soil and Tillage Research*, 218. <https://doi.org/10.1016/j.still.2021.105295>. Article 105295.
- Govaerts, B., Verhulst, N., Castellanos-Navarrete, A., Sayre, K. D., Dixon, J., & Dendooven, L. (2009). Conservation agriculture and soil carbon sequestration: Between myth and farmer reality. *Critical Reviews in Plant Sciences*, 28(3), 97–122. <https://doi.org/10.1080/07352680902776358>
- Jiang, Y., Xie, H., & Chen, Z. (2021). Relationship between the amounts of surface corn stover mulch and soil mesofauna assemblage varies with the season in cultivated areas of northeastern China. *Soil and Tillage Research*, 213. <https://doi.org/10.1016/j.still.2021.105091>. Article 105091.
- Kassam, A. H., Friedrich, T., Shaxson, F., & Pretty, J. (2009). The spread of conservation agriculture: Justification, sustainability and uptake. *International Journal of Agricultural Sustainability*, 7(4), 292–320.
- Kumar, S., Kadono, A., Lal, R., & Dick, W. (2012). Long-term no-till impacts on organic carbon and properties of two contrasting soils and corn yields in Ohio. *Soil Science Society of America Journal*, 76, 1798–1809. <https://doi.org/10.2136/sssaj2012.0055>
- Lee, M. J., & Kwak, H. G. (2023). Impact simulations for high-performance fiber-reinforced cement composites using a coupled finite element and smoothed particle Galerkin method. *International Journal of Damage Mechanics*, 32(3), 424–441. <https://doi.org/10.1177/10567895221146578>
- Li, H., & Schindler, C. (2012). Application of analytical and finite element method in tyre-soil modelling. *International Journal of Heavy Vehicle Systems*, 19(4), 333–354. <https://doi.org/10.1504/IJHVS.2012.049846>
- Li, M., Xu, S., Yang, Y., Guo, L., & Tong, J. (2017). A 3D simulation model of corn stubble cutting using finite element method. *Soil and Tillage Research*, 166, 43–51. <https://doi.org/10.1016/j.still.2016.10.003>
- Li, X., Zhu, L., & Gong, S. (2022). Soil-cutting simulation and dual-objective optimization on tillage process parameters of micro-tiller by smoothed particle Galerkin modeling and genetic algorithm. *Computers and Electronics in Agriculture*, 198. <https://doi.org/10.1016/j.compag.2022.107021>. Article 107021.
- LSTC. (2018). *LS-DYNA r11.0 Keyword user's manual*. Livermore Software Technology Corporation.
- Ma'ruf, M. F. (2012). Shear strength of Apus bamboo root reinforced soil. *Ecological Engineering*, 41, 84–86. <https://doi.org/10.1016/j.ecoleng.2012.01.003>
- Melland, A. R., Antille, D. L., & Dang, Y. P. (2017). Effects of strategic tillage on short-term erosion, nutrient loss in runoff and greenhouse gas emissions. *Soil Research*, 55(3), 201–214. <https://doi.org/10.1071/SR16136>
- Mickovski, S. B., Stokes, A., Beek, R. V., Ghensem, M., & Fourcaud, T. (2011). Simulation of direct shear tests on rooted and non-rooted soil using finite element analysis. *Ecological Engineering*, 37, 1523–1532. <https://doi.org/10.1016/j.ecoleng.2011.06.001>
- Rashidi, M., & Gholami, M. (2010). Prediction of soil sinkage by multiple loadings using the finite element method. *International Journal of Agriculture and Biology*, 12(6), 911–915.
- Schenk, H. J., & Jackson, R. B. (2002). Rooting depths, lateral root spreads and below-ground/above-ground allometries of plants in water-limited ecosystems. *Journal of Ecology*, 90(3), 480–494. <https://doi.org/10.1046/j.1365-2745.2002.00682.x>
- Seitz, S., Goebes, P., Puerta, V. L., Pereira, E. I. P., Wittwer, R., Six, J., et al. (2019). Conservation tillage and organic farming reduce soil erosion. *Agronomy for Sustainable Development*, 39(4), 1–10. <https://doi.org/10.1007/s13593-018-0545-z>

- Stockburger, E., Zhang, W., Wester, H., Rosenbusch, D., & Behrens, B.-A. (2023). Process analyses of friction drilling using the smoothed particle Galerkin method. *International Journal of Material Forming*, 16(1), 14. <https://doi.org/10.1007/s12289-022-01733-0>
- Su, X., Zhou, Z., Liu, Jun'e, Wang, P., Liu, J., Li, Q., & Zhao, F. (2022). The role of roots traits of climax community species to shear strength in the Loess Hilly Region, China. *Soil and Tillage Research*, 221. <https://doi.org/10.1016/j.still.2022.105417>. Article 105417.
- Tagar, A. A., Changying, J., Adamowski, J., Malard, J., Qi, C. S., Qishuo, D., & Abbasi, N. A. (2015). Finite element simulation of soil failure patterns under soil bin and field testing conditions. *Soil and Tillage Research*, 145, 157–170. <https://doi.org/10.1016/j.still.2014.09.006>
- Tanaka, H., Momozu, M., Oida, A., & Yamazaki, M. (2000). Simulation of soil deformation and resistance at bar penetration by the Distinct Element Method. *Journal of Terramechanics*, 37(1), 41–56. [https://doi.org/10.1016/S0022-4898\(99\)00013-0](https://doi.org/10.1016/S0022-4898(99)00013-0)
- Temgoua, A. G. T., Kokutse, N. K., & Kavazović, Z. (2016). Influence of forest stands and root morphologies on hillslope stability. *Ecological Engineering*, 95, 622–634. <https://doi.org/10.1016/j.ecoleng.2016.06.073>
- Tian, Y. J., Sang, Y. C., & Liu, J. (2022). A numerical model for rock cutting with diamond circular saw blade based on smoothed particle galerkin method. *Mathematical Problems in Engineering*, 2022, 1–17. <https://doi.org/10.1155/2022/2036301>
- Tomobe, H., Fujisawa, K., & Murakami, A. (2019). Experiments and FE-analysis of 2-D root-soil contact problems based on node-to-segment approach. *Soils and Foundations*, 59(6), 1860–1874. <https://doi.org/10.1016/j.sandf.2019.08.003>
- Tomobe, H., Fujisawa, K., & Murakami, A. (2021). A mohr-coulomb-vilar model for constitutive relationship in root-soil interface under changing suction. *Soils and Foundations*, 61(3), 815–835. <https://doi.org/10.1016/j.sandf.2021.03.005>
- Ucgul, M., Fielke, J. M., & Saunders, C. (2014). 3D DEM tillage simulation: Validation of a hysteretic spring (plastic) contact model for a sweep tool operating in a cohesionless soil. *Soil and Tillage Research*, 144, 220–227. <https://doi.org/10.1016/j.still.2013.10.003>
- Ucgul, M., Saunders, C., & Fielke, J. M. (2017). Discrete element modelling of tillage forces and soil movement of a one-third scale mouldboard plough. *Biosystems Engineering*, 155, 44–54. <https://doi.org/10.1016/j.biosystemseng.2016.12.002>
- Upadhyaya, P., & Kumar, S. (2015). Micromechanics of stress transfer through the interphase in fiber-reinforced composites. *Mechanics of Materials*, 89, 190–201. <https://doi.org/10.1016/j.mechmat.2015.06.012>
- Upadhyaya, S. K., Rosa, U. A., & Wulfsohn, D. (2002). Application of the finite element method in agricultural soil mechanics. *Advances in Soil Dynamics*, 2, 117–153. <https://doi.org/10.13031/2013.9451>
- Vannoppen, W., Vanmaercke, M., De Baets, S., & Poesen, J. (2015). A review of the mechanical effects of plant roots on concentrated flow erosion rates. *Earth-Science Reviews*, 150, 666–678. <https://doi.org/10.1016/j.earscirev.2015.08.011>
- Wardle, D. A., Bardgett, R. D., Klironomos, J. N., Setälä, H., van der Putten, W. H., & Wall, D. H. (2004). Ecological linkages between aboveground and belowground biota. *Science*, 304(5677), 1629–1633. <https://doi.org/10.1126/science.1094875>
- Wu, T. H., Beal, P. E., & Lan, C. (1988). In-situ test of soil-root systems. *Journal of Geotechnical Engineering*, 114(12), 1376–1394. [https://doi.org/10.1061/\(ASCE\)0733-9410\(1988\)114:12\(1376\)](https://doi.org/10.1061/(ASCE)0733-9410(1988)114:12(1376))
- Wu, C. T., Bui, T. Q., Wu, Y., Luo, T.-L., Wang, M., Liao, C.-C., et al. (2018). Numerical and experimental validation of a particle Galerkin method for metal grinding simulation. *Computational Mechanics*, 61, 365–383. <https://doi.org/10.1007/s00466-017-1456-6>
- Wu, L., Cheng, P., Zhou, J., & Li, S. (2022). Analytical solution of rainfall infiltration for vegetated slope in unsaturated soils considering hydro-mechanical effects. *Catena*, 217, Article 106472. <https://doi.org/10.1016/j.catena.2022.106472>
- Wu, C.-T., Chi, S.-W., Koishi, M., & Wu, Y. (2016). Strain gradient stabilization with dual stress points for the meshfree nodal integration method in inelastic analyses. *International Journal for Numerical Methods in Engineering*, 107(1), 3–30. <https://doi.org/10.1002/nme.5147>
- Wu, C.-T., Koishi, M., & Hu, W. (2015). A displacement smoothing induced strain gradient stabilization for the meshfree Galerkin nodal integration method. *Computational Mechanics*, 56(1), 19–37. <https://doi.org/10.1007/s00466-015-1153-2>
- Wu, Y., & Wu, C. T. (2018). Simulation of impact penetration and perforation of metal targets using the smoothed particle galerkin method. *Journal of Engineering Mechanics*, 144(8). [https://doi.org/10.1061/\(ASCE\)EM.1943-7889.0001470](https://doi.org/10.1061/(ASCE)EM.1943-7889.0001470). Article 04018057.
- Wu, C.-T., Wu, Y., Crawford, J. E., & Magallanes, J. M. (2017). Three-dimensional concrete impact and penetration simulations using the smoothed particle Galerkin method. *International Journal of Impact Engineering*, 106, 1–17. <https://doi.org/10.1016/j.ijimpeng.2017.03.005>
- Wu, Y., Wu, C.-T., & Hu, W. (2017). Modeling of ductile failure in destructive manufacturing processes using the smoothed particle galerkin method. In *Proceedings of the China LS-DYNA users conference* (pp. 23–25). Shanghai, China.
- Wu, C.-T., Wu, Y., Lyu, D., Pan, X., & Hu, W. (2020). The momentum-consistent smoothed particle Galerkin (MC-SPG) method for simulating the extreme thread forming in the flow drill screw-driving process. *Computational Particle Mechanics*, 7(2), 177–191. <https://doi.org/10.1007/s40571-019-00235-2>
- Yan, Z.-x., Song, Y., Jiang, P., & Wang, H.-y. (2010). Mechanical analysis of interaction between plant roots and rock and soil mass in slope vegetation. *Applied Mathematics and Mechanics*, 31(5), 617–622. <https://doi.org/10.1007/s10483-010-0509-9>
- Yang, M., Défossez, P., Danjon, F., & Fourcaud, T. (2014). Tree stability under wind: Simulating uprooting with root breakage using a finite element method. *Annals of Botany*, 114, 695–709. <https://doi.org/10.1093/aob/mcu122>
- Yuan, Y., Wang, J., Zhang, X., & Zhao, S. (2023). Effect of rotary speed on soil and straw throwing process by stubble-crushing blade for strip tillage using DEM-CFD. *Agriculture*, 13(4), 877. <https://doi.org/10.3390/agriculture13040877>
- Zhang, S., Chen, X., Jia, S., Liang, A., Zhang, X., Yang, X., et al. (2015). The potential mechanism of long-term conservation tillage effects on maize yield in the black soil of Northeast China. *Soil and Tillage Research*, 154, 84–90. <https://doi.org/10.1016/j.still.2015.06.002>
- Zhang, B., Han, Q., Zhang, J., Han, Z., Niu, S., & Ren, L. (2020). Advanced bio-inspired structural materials: Local properties determine overall performance. *Materials Today*, 41, 177–199. <https://doi.org/10.1016/j.mattod.2020.04.009>
- Zhang, S. X., Li, Q., Zhang, X. P., Wei, K., Chen, L. J., & Liang, W. L. (2012). Effects of conservation tillage on soil aggregation and aggregate binding agents in black soil of Northeast China. *Soil and Tillage Research*, 124, 196–202. <https://doi.org/10.1016/j.still.2012.06.007>
- Zhang, S., Zhao, H., Wang, X., Dong, J., Zhao, P., Yang, F., et al. (2023). Discrete element modeling and shear properties of the maize stubble-soil complex. *Computers and Electronics in Agriculture*, 204. <https://doi.org/10.1016/j.compag.2022.107519>. Article 107519.